Journal of Applied Mechanics and Technical Physics, Vol. 48, No. 5, pp. 755–765, 2007

REFINED GEOMETRICALLY NONLINEAR FORMULATION OF A THIN-SHELL TRIANGULAR FINITE ELEMENT

V. V. Kuznetsov and S. V. Levyakov

UDC 539.3

A refined geometrically nonlinear formulation of a thin-shell finite element based on the Kirchhoff–Love hypotheses is considered. Strain relations, which adequately describe the deformation of the element with finite bending of its middle surface, are obtained by integrating the differential equation of a planar curve. For a triangular element with 15 degrees of freedom, a cost-effective algorithm is developed for calculating the coefficients of the first and second variations of the strain energy, which are used to formulate the conditions of equilibrium and stability of the discrete model of the shell. Accuracy and convergence of the finite-element solutions are studied using test problems of nonlinear deformation of elastic plates and shells.

Key words: *thin shell, nonlinear deformation, finite-element method, invariants, kinematic group, planar curve.*

Introduction. Considerable advances in solving complex problems of nonlinear mechanics of thin-walled shell structures have been made owing to methods of discrete analysis, among which the finite-element method has been the most popular one. As applied to analysis of plates and shells, two trends of evolution of this method can be distinguished: the approach based on the Kirchhoff–Love hypotheses and that based on the Timoshenko and Reissner–Mindlin theory of plates and shells, which takes into account the transverse shear strains. The dominant trend in studying finite-element shell models is related to the Reissner–Mindlin model, which relaxes the continuity condition for the approximating functions. As the shell thickness decreases, however, the solution obtained by low-order finite elements exhibits a poor convergence rate with respect to the number of finite elements because of the "locking" effects. Attempts to remove this effect lead to very involved formulations (see, e.g. [1]).

The finite elements based on the Kirchhoff–Love hypotheses are free of "locking" effects, but their construction requires using high-order approximating polynomials, which leads to an increase in the computational work and complicates computational algorithms.

It is of interest to consider the question of refining simple finite-element models of a thin shell without increasing the number of degrees of freedom. The traditional approach to constructing finite elements is to establish a relation between the displacement fields within an element and nodal parameters using shape functions. In the process, the strain-tensor components are obtained by differentiating the shape functions. Alternative approaches such as methods of geometrical and mechanical analogies are seldom used. In the present paper, for solving geometrically nonlinear problems, an approach of this kind is proposed for constructing a finite element of a thin shell, which is based on the expression for the strain energy in terms of invariants of the strain-rate tensors and changes in curvature of the shell middle surface [2], the kinematic group theory [3], and the integration of the differential equation of a planar curve [4]. The use of these notions allows one to refine the formulation of basic relations without increasing the number of degrees of freedom and develop a cost-effective algorithm for calculating the components of the first and second variations of the finite element strain energy, which are required to formulate the conditions of equilibrium and stability of the discrete model of the shell. A triangular 15 degrees of freedom

Novosibirsk State Technical University, Novosibirsk 630092; vku1952@yandex.ru; lest@sibmail.ru. Translated from Prikladnaya Mekhanika i Tekhnicheskaya Fizika, Vol. 48, No. 5, pp. 160–172, September–October, 2007. Original article submitted April 25, 2006; revision submitted August 31, 2006.

finite element is constructed. A specific feature of the approach proposed is that, for the initial and deformed states, the shell geometry is determined by the coordinates and direction cosines of the normal vector to the middle surface at each node of the finite-element model.

1. Strain Energy of the Shell Element. We consider a triangular finite element of a thin isotropic shell. The strains of the shell are assumed to be small, but no restrictions are imposed on the magnitude of displacements and rotations. We assume that the middle surface of the element is isometric to a planar triangle with sides l_m ($m = 1, 2, 3$). As the physical components of the Green strain tensor, we use the normal strains ε_m of the fibers directed along the triangle sides. Assuming that the shell obeys the Kirchhoff–Love hypotheses $\varepsilon_m^z = \varepsilon_m + z\varkappa_m$ and $\sigma_z = 0$ (z is the normal coordinate to the middle surface, σ_z is the normal stress, and $\varkappa_m$ is the change in curvature of the middle surface in the corresponding direction), we write the strain energy of the shell element as

$$\Pi = \frac{1}{2}\int\limits_F B(I_\varepsilon^2 - 2(1-\nu)I_{\varepsilon\varepsilon})\,dF + \frac{1}{2}\int\limits_F D(I_\varkappa^2 - 2(1-\nu)I_{\varkappa\varkappa})\,dF, \tag{1.1}$$

where

$$I_\varepsilon = (\varepsilon_m l_m^2 l^2 - 2\varepsilon_m l_m^4)/(8F^2), \qquad I_{\varepsilon\varepsilon} = ((\varepsilon_m l_m^2)^2 - 2\varepsilon_m^2 l_m^4)/(16F^2),$$

$$I_\varkappa = (\varkappa_m l_m^2 l^2 - 2\varkappa_m l_m^4)/(8F^2), \qquad I_{\varkappa\varkappa} = ((\varkappa_m l_m^2)^2 - 2\varkappa_m^2 l_m^4)/(16F^2),$$

$$F^2 = (l^4 - 2l_m^2 l_m^2)/16, \qquad l^2 = l_m l_m, \qquad B = Eh/(1-\nu^2), \quad D = Bh^2/12,$$

I_ε and $I_{\varepsilon\varepsilon}$ ($I_\varkappa$ and $I_{\varkappa\varkappa}$) are the first and second strain (middle-surface curvature change) invariants, respectively, F is the area of the middle surface of the triangular element, and E, ν, and h are the elastic modulus, Poisson's ratio, and shell thickness, respectively; summation is performed over the subscript $m = 1, 2, 3$.

2. Kinematic Group of The Shell Element. The kinematic group of the triangular shell element [3] is characterized by the nodal radius vectors $\boldsymbol{r}_i$ and adjoined unit vectors $\boldsymbol{n}_i$ normal to its middle surface. The following parameters are used as independent components of the generalized metric tensor of the group:

$$e_i = (\boldsymbol{r}_k - \boldsymbol{r}_j)^2/(2l_i^2), \qquad \psi_{1i} = \boldsymbol{n}_i(\boldsymbol{r}_j - \boldsymbol{r}_i)/l_k, \qquad \psi_{2i} = \boldsymbol{n}_i(\boldsymbol{r}_i - \boldsymbol{r}_k)/l_j. \tag{2.1}$$

Here and below, the subscripts i, j, and k take the values 1, 2, and 3 by cyclic permutation, and the lengths l_i have the meaning of normalization factors introduced for convenience. Replacing $\boldsymbol{r}_i$ and $\boldsymbol{n}_i$ by $\boldsymbol{r}_i^*$ and $\boldsymbol{n}_i^*$, respectively, in formulas (2.1), one obtains the components of the generalized metric tensor of the kinematic group for a deformed state (the superscript asterisk denotes the quantities that refer to a deformed state). In the process, the normalization factors remain unchanged.

3. Strain Model of the Shell Element. We assume that the strains ε_i of the middle surface are constant and determined in terms of the strains of the triangular element sides, while the curvature changes $\varkappa_i$ can be expressed in terms of rotations of the normal in the normal plane passing through the corresponding nodes of the element. We assume that, for the initial and deformed states, the intersection of the middle surface and the normal plane defines a curve whose shape is close to a circular arc. Moreover, we ignore the deviation of the unit normal vectors at the nodes from the plane that passes through these nodes [5]. It should be noted that the assumptions accepted are valid for reasonably small elements but ensure a higher approximation order, as compared to the asymptotic relations [6].

We write the differential equation of a planar curve (side of the triangular element in the initial state)

$$\boldsymbol{n}' = \varkappa\boldsymbol{r}', \tag{3.1}$$

where $\boldsymbol{r}$ is the radius vector of the curve, $\boldsymbol{n}$ is the normal vector, and $\varkappa$ is the curvature of the curve; the prime denotes differentiation with respect to the natural coordinate. Integrating Eq. (3.1) from 0 to l_i for $\varkappa = \text{const}$ between the nodes j and k, we obtain

$$\boldsymbol{n}_k - \boldsymbol{n}_j = (\varphi_i/l_i)(\boldsymbol{r}_k - \boldsymbol{r}_j), \tag{3.2}$$

where $\varkappa = \varphi_i/l_i$ and φ_i is the angle between the vectors $\boldsymbol{n}_j$ and $\boldsymbol{n}_k$ (opening angle). Squaring both sides of Eq. (3.2), we obtain

$$2(1 - \cos\varphi_i) = (\varphi_i^2/l_i^2)(\boldsymbol{r}_k - \boldsymbol{r}_j)^2. \tag{3.3}$$

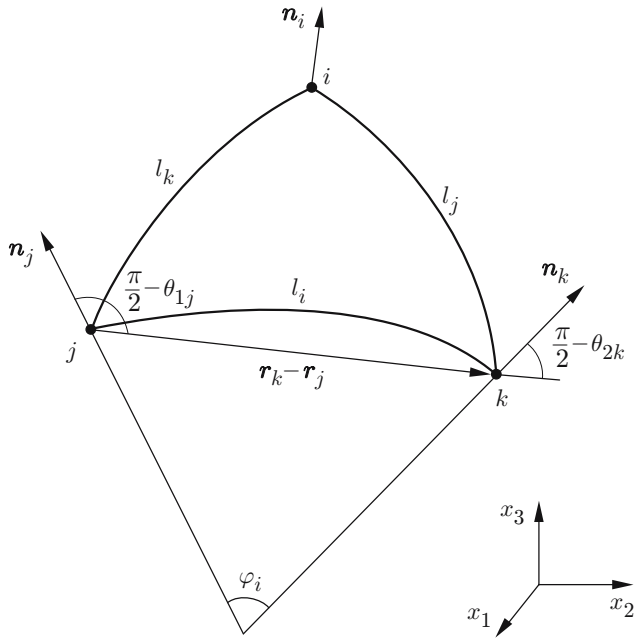

Fig. 1. Finite element of a shell.

Writing Eq. (3.3) for a deformed state and setting $l_i^{*2} = (1 + 2\varepsilon_i)l_i^2$ by definition of the physical components of the Green tensor, with allowance for the first relation of (2.1), we obtain the strain

$$\varepsilon_i = (2e_i^* G(\varphi_i^*) - 1)/2, \qquad G(\varphi) = \varphi^2/[2(1 - \cos\varphi)].$$

Using Eq. (3.2), we obtain expressions for the opening angles

$$\varphi_i = \theta_{2k} - \theta_{1j}, \qquad \theta_{1i} = \psi_{1i}/(2e_k), \qquad \theta_{2i} = \psi_{2i}/(2e_j). \tag{3.4}$$

Here $\pi/2 - \theta_{mn}$ is the angle in the normal plane between the normal vector at the nth node and the secant passing through the nodes (Fig. 1). The rotations of the normal vector in the normal plane due to element deformation are

$$\vartheta_{mn} = \theta_{mn}^* - \theta_{mn}.$$

Since the vectors $\boldsymbol{r}_i$ and $\boldsymbol{n}_i$ are known for the initial state, the lengths of the triangle sides are determined using relations (3.3) and (3.4):

$$l_i^2 = (\boldsymbol{r}_k - \boldsymbol{r}_j)^2 G(\varphi_i), \qquad \varphi_i = \arccos\{1 - a_i^2/[2(\boldsymbol{r}_k - \boldsymbol{r}_j)^2]\}, \qquad a_i = (\boldsymbol{r}_k - \boldsymbol{r}_j)(\boldsymbol{n}_k - \boldsymbol{n}_j).$$

To approximate $\varkappa_i$, we use the following law of variation of the curvature of a simply supported beam under the action of bending moments applied to its ends [4]:

$$\varkappa_i = (\vartheta_{2k} - \vartheta_{1j})/l_i + 3(\vartheta_{2k} + \vartheta_{1j})(L_k - L_j)/l_i. \tag{3.5}$$

Here L_k are the area coordinates [7], the first term valid for all values of ϑ_{mn} takes into account the constant curvature-change component, and the second term (which was ignored in determining ε_i) describes a small deviation of the shape of the normal section from the circular arc. It should be noted that the expression for the strain energy (1.1) allows one to avoid constructing the area coordinates and, hence, reduce the number of arithmetic operations in calculating the element stiffness matrix.

The relations given above imply that the quantities characterizing the deformed state of the shell element can be expressed in terms of the metric tensors of the kinematic group (2.1) for the initial and deformed states. Hence, the variational problem for the finite element reduces to the variational problem for the kinematic group [3].

4. Variations of the Strain Energy. To formulate the conditions of equilibrium and stability and to construct an iterative solution algorithm, it is necessary to calculate the first and second variations of the strain energy of the discrete system. For algorithmic computations, we introduce three levels of varied parameters [8]:

$$\boldsymbol{u}_{(1)} = (\varepsilon_1, \varepsilon_2, \varepsilon_3, \vartheta_{23}, \vartheta_{12}, \vartheta_{21}, \vartheta_{13}, \vartheta_{22}, \vartheta_{11})^{\mathrm{t}},$$

$$\boldsymbol{u}_{(2)} = (e_1^*, e_2^*, e_3^*, \psi_{23}^*, \psi_{12}^*, \psi_{21}^*, \psi_{13}^*, \psi_{22}^*, \psi_{11}^*)^{\mathrm{t}}, \tag{4.1}$$

$$\boldsymbol{u}_{(3)} = \boldsymbol{q} = (\boldsymbol{q}_1^{\mathrm{t}}, \boldsymbol{q}_2^{\mathrm{t}}, \boldsymbol{q}_3^{\mathrm{t}})^{\mathrm{t}}, \qquad \boldsymbol{q}_m^{\mathrm{t}} = (x_{1m}^*, x_{2m}^*, x_{3m}^*, \omega_{1m}, \omega_{2m}) \quad (m = 1, 2, 3).$$

Here x_{mn}^* are the components of the radius vector $\boldsymbol{r}_n^*$ and ω_{mn} are the components of the rotation vector of the normal vector $\boldsymbol{n}_n^*$; the subscript in parentheses refers to the level number. At any variation level, the first and second variations of the strain energy have the form

$$\delta\Pi = \delta\boldsymbol{u}_{(m)}^{\mathrm{t}}\boldsymbol{g}_{(m)}, \qquad \delta^2\Pi = \delta\boldsymbol{u}_{(m)}^{\mathrm{t}}H_{(m)}\delta\boldsymbol{u}_{(m)}$$

($\boldsymbol{g}_{(m)}$ and $H_{(m)}$ are the gradient and Hess matrix of the mth level). To calculate $\boldsymbol{g} = \boldsymbol{g}_{(3)}$ and $H = H_{(3)}$ (the level of the generalized coordinates of the kinematic group), we use the recursive relations [8]:

$$\boldsymbol{g}_{(m+1)} = u'_{(m)}\boldsymbol{g}_{(m)}, \qquad H_{(m+1)} = u'_{(m)}H_{(m)}u'^{\mathrm{t}}_{(m)} + g_{(m)s}u''_{(m)s},$$
$$m = 1, 2, \qquad s = 1, \ldots, 9. \tag{4.2}$$

Here $g_{(m)s}$ are the components of the vector $\boldsymbol{g}_{(m)}$, $u'_{(m)}$ and $u''_{(m)s}$ are the matrices of the first and second partial derivatives of the mth level variables with respect to the $(m+1)$th level variables, respectively; summation is performed over s. As the strain energy at the first level has the form

$$\Pi = \boldsymbol{u}_{(1)}^{\mathrm{t}}K\boldsymbol{u}_{(1)}/2$$

(K is the stiffness matrix), the initial values in the recursive formulas (4.2) are given by

$$\boldsymbol{g}_{(1)} = K\boldsymbol{u}_{(1)}, \qquad H_{(1)} = K.$$

Using relations (1.1), (2.1), and (3.5), we obtain the expression for the element stiffness matrix:

$$K = \begin{pmatrix} K_\varepsilon & 0 \\ 0 & K_\vartheta \end{pmatrix}, \qquad K_\varepsilon = BFA, \qquad A = \boldsymbol{\tau}\boldsymbol{\tau}^{\mathrm{t}} - \frac{1-\nu}{8F^2}\,(\boldsymbol{\mu}\boldsymbol{\mu}^{\mathrm{t}} - \rho), \tag{4.3}$$

where

$$\boldsymbol{\tau}^{\mathrm{t}} = (l^2l_1^2 - 2l_1^4, l^2l_2^2 - 2l_2^4, l^2l_3^2 - 2l_3^4)/(8F^2), \qquad \rho_{mm} = 2l_m^4, \qquad \boldsymbol{\mu}^{\mathrm{t}} = (l_1^2, l_2^2, l_3^2),$$

$$K_\vartheta = D\int\limits_F M(L_1, L_2, L_3)\,dF, \qquad M(L_1, L_2, L_3) = C^{\mathrm{t}}AC;$$

nonzero components are given for the matrix ρ. Nonzero components of the 3×6 matrix C are given by

$$C_{11} = (1 + 3(L_3 - L_2))/l_1, \qquad C_{12} = -(1 + 3(L_2 - L_3))/l_1,$$

$$C_{23} = (1 + 3(L_1 - L_3))/l_2, \qquad C_{24} = -(1 + 3(L_3 - L_1))/l_2, \tag{4.4}$$

$$C_{35} = (1 + 3(L_2 - L_1))/l_3, \qquad C_{36} = -(1 + 3(L_1 - L_2))/l_3.$$

As expressions (4.4) are linear for the area coordinates, the components of the matrix $M(L_1, L_2, L_3)$ are quadratic functions of the area coordinates. In this case, the integral in (4.3) can be evaluated exactly by the formula [7]

$$\int\limits_F M(L_1, L_2, L_3)\,dF = \frac{F}{3}\Big(M\Big(\frac{1}{2}, \frac{1}{2}, 0\Big) + M\Big(0, \frac{1}{2}, \frac{1}{2}\Big) + M\Big(\frac{1}{2}, 0, \frac{1}{2}\Big)\Big).$$

Nonzero components of the matrix $u'_{(1)}$ are given by

$$\frac{\partial\varepsilon_i}{\partial e_i^*} = G(\varphi_i^*) - \varphi_i^*G'(\varphi_i^*), \qquad \frac{\partial\varepsilon_i}{\partial\psi_{2k}^*} = -\frac{\partial\varepsilon_i}{\partial\psi_{1j}^*} = \frac{1}{2}\,G'(\varphi_i^*),$$

$$\frac{\partial\vartheta_{2k}}{\partial e_i^*} = -\frac{1}{2e_i^{*2}}\,\psi_{2k}^*, \qquad \frac{\partial\vartheta_{1j}}{\partial e_i^*} = -\frac{1}{2e_i^{*2}}\,\psi_{1j}^*,$$

$$\frac{\partial\vartheta_{2k}}{\partial\psi^*_{2k}}=\frac{\partial\vartheta_{1j}}{\partial\psi^*_{1j}}=\frac{1}{2e^*_i},\qquad G'(\varphi)=\frac{\varphi(1-\cos\varphi-(1/2)\varphi\sin\varphi)}{(1-\cos\varphi)^2}.$$

Nonzero components of the matrices $u''_{(1)s}$ $(s=1,\ldots,9)$ are given by

$$\frac{\partial^2\varepsilon_i}{\partial e^{*2}_i}=\frac{\varphi^{*2}_i}{e^*_i}G''(\varphi^*_i),\qquad \frac{\partial^2\varepsilon_i}{\partial e^*_i\,\partial\psi^*_{2k}}=-\frac{\partial^2\varepsilon_i}{\partial e^*_i\,\partial\psi^*_{1j}}=-\frac{\varphi^*_i}{2e^*_i}\,G''(\varphi^*_i),$$

$$\frac{\partial^2\varepsilon_i}{\partial\psi^{*2}_{2k}}=\frac{\partial^2\varepsilon_i}{\partial\psi^{*2}_{1j}}=-\frac{\partial^2\varepsilon_i}{\partial\psi^*_{2k}\,\partial\psi^*_{1j}}=\frac{1}{4e^*_i}\,G''(\varphi^*_i),$$

$$\frac{\partial^2\vartheta_{2k}}{\partial e^{*2}_i}=\frac{1}{e^{*3}_i}\,\psi^*_{2k},\qquad \frac{\partial^2\vartheta_{1j}}{\partial e^{*2}_i}=\frac{1}{e^{*3}_i}\,\psi^*_{1j},\qquad \frac{\partial^2\vartheta_{2k}}{\partial e^*_i\,\partial\psi^*_{2k}}=\frac{\partial^2\vartheta_{1j}}{\partial e^*_i\,\partial\psi^*_{1j}}=-\frac{1}{2e^{*2}_i},$$

$$G''(\varphi)=\frac{1-\cos\varphi-2\varphi\sin\varphi+\varphi^2(1+(1/2)\cos\varphi)}{(1-\cos\varphi)^2}.$$

It is worth noting that the expressions for the function $G(\varphi)$ and its derivatives contain uncertainties of the type $(0/0)$ as $\varphi\to0$. For small values of the parameter $|\varphi|<0.1$, we use the Taylor series expansions

$$G(\varphi)=1+\frac{\varphi^2}{12}+\frac{\varphi^4}{240}+O(\varphi^6),\qquad G'(\varphi)=\frac{\varphi}{6}+\frac{\varphi^3}{60}+O(\varphi^5),\qquad G''(\varphi)=\frac{1}{6}+\frac{\varphi^2}{20}+O(\varphi^4).$$

The partial derivatives of the second-level variables with respect to the third-level variables (4.1), which determine the matrices $u'_{(2)}$ and $u''_{(2)s}$ $(s=1,\ldots,9)$, are given by

$$\frac{\partial e^*_i}{\partial x^*_{mk}}=-\frac{\partial e^*_i}{\partial x^*_{mj}}=\frac{1}{l^2_i}\,(x^*_{mk}-x^*_{mj}),\qquad \frac{\partial\psi^*_{1i}}{\partial x^*_{mj}}=-\frac{\partial\psi^*_{1i}}{\partial x^*_{mi}}=\frac{\lambda^*_{3mi}}{l_k},$$

$$\frac{\partial\psi^*_{2i}}{\partial x^*_{mi}}=-\frac{\partial\psi^*_{2i}}{\partial x^*_{mk}}=\frac{\lambda^*_{3mi}}{l_j},\qquad \frac{\partial\psi^*_{1i}}{\partial\omega_{mi}}=\frac{1}{l_k}\,\lambda^*_{mni}(x^*_{nj}-x^*_{ni}),\qquad \frac{\partial\psi^*_{2i}}{\partial\omega_{mi}}=\frac{1}{l_j}\,\lambda^*_{mni}(x^*_{ni}-x^*_{nk}),$$

$$\frac{\partial^2 e^*_i}{\partial x^{*2}_{mk}}=\frac{\partial^2 e^*_i}{\partial x^{*2}_{mj}}=-\frac{\partial^2 e^*_i}{\partial x^*_{mk}\partial x^*_{mj}}=\frac{1}{l^2_i},\qquad \frac{\partial^2\psi^*_{1i}}{\partial x^*_{mj}\,\partial\omega_{si}}=-\frac{\partial^2\psi^*_{1i}}{\partial x^*_{mi}\,\partial\omega_{si}}=\frac{\lambda^*_{smi}}{l_k},\tag{4.5}$$

$$\frac{\partial^2\psi^*_{2i}}{\partial x^*_{mi}\,\partial\omega_{si}}=-\frac{\partial^2\psi^*_{2i}}{\partial x^*_{mk}\,\partial\omega_{si}}=\frac{\lambda^*_{smi}}{l_j},$$

$$\frac{\partial^2\psi^*_{1i}}{\partial\omega^2_{mi}}=-\frac{1}{l_k}\,\lambda^*_{3ni}(x^*_{nj}-x^*_{ni}),\qquad \frac{\partial^2\psi^*_{2i}}{\partial\omega^2_{mi}}=-\frac{1}{l_j}\,\lambda^*_{3ni}(x^*_{ni}-x^*_{nk}).$$

Here summation is performed over $n=1,2,3$; λ^*_{jni} are the direction cosines of the vectors $\boldsymbol{t}^*_{1i}$, $\boldsymbol{t}^*_{2i}$, and $\boldsymbol{t}^*_{3i}=\boldsymbol{n}^*_i$ at the ith node, which form a right-handed triad of orthogonal vectors $\boldsymbol{t}^*_{mi}=(\lambda^*_{m1i},\lambda^*_{m2i},\lambda^*_{m3i})^{\mathrm{t}}$ $(i,m=1,2,3)$.

To calculate shells using the approach considered above, one should specify, as the initial data, the coordinates x_{si} and the direction cosines of the normal vectors λ_{3si} at nodes of the finite-element mesh. It should be noted that the unit vectors $\boldsymbol{t}^*_{1i}$ and $\boldsymbol{t}^*_{2i}$ tangent to the deformed shell middle surface are of auxiliary character and serve to calculate the variations of the normal vectors according to formulas (4.5). These vectors can easily be constructed for a given normal vector $\boldsymbol{n}^*_i$.

5. Solution Algorithm. For a finite-element assemblage, the equations of equilibrium can be written in the matrix form as

$$\boldsymbol{g}-\lambda\boldsymbol{P}=0.\tag{5.1}$$

Here $\boldsymbol{P}$ is the vector of the generalized external forces with a linear potential and λ is the loading parameter. Equations (5.1) are solved by the Newton–Raphson method combined with the step-by-step variation in the loading parameter according to the scheme

$$H^{(p)}\,\delta\boldsymbol{q}^{(p)}\;+\;\boldsymbol{g}^{(p)}-\lambda\boldsymbol{P}=0,$$

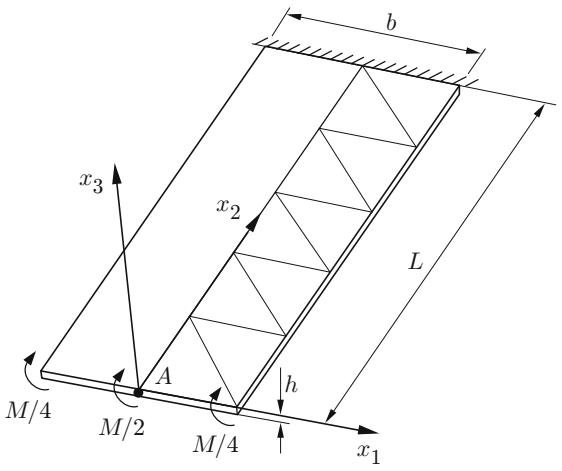

Fig. 2. Cantilever strip under pure bending.

where the superscript in parentheses enumerates iterations. Stability of equilibrium states determined is investigated using the Sylvester criterion for the matrix H. During iterations, new values of the nodal unknowns are determined by the formulas [9]

$$\boldsymbol{r}_s^{*(p+1)} = \boldsymbol{r}_s^{*(p)} + \delta\boldsymbol{r}_s^{*(p)}, \qquad \boldsymbol{n}_s^{*(p+1)} = a_1\boldsymbol{n}_s^{*(p)} + a_2(\boldsymbol{t}_{1s}^{*(p)}\delta\omega_{1s}^{(p)} + \boldsymbol{t}_{2s}^{*(p)}\delta\omega_{2s}^{(p)}),$$

$$\boldsymbol{t}_{ms}^{*(p+1)} = \boldsymbol{t}_{ms}^{*(p)} - \delta\omega_{ms}[a_2\boldsymbol{n}_s^{*(p)} + a_3(\boldsymbol{t}_{1s}^{*(p)}\delta\omega_{1s}^{(p)} + \boldsymbol{t}_{2s}^{*(p)}\delta\omega_{2s}^{(p)})],$$

$$\delta\omega_s^{(p)} = (\delta\omega_{1m}^{(p)2} + \delta\omega_{2m}^{(p)2})^{1/2}, \quad a_1 = \cos\delta\omega_s^{(p)}, \quad a_2 = \frac{\sin\delta\omega_s^{(p)}}{\delta\omega_s^{(p)}}, \quad a_3 = \frac{1-\cos\delta\omega_s^{(p)}}{\delta\omega_s^{(p)2}}.$$

Formulas for the coefficients a_2 and a_3 contain uncertainties of the type (0/0) as $\delta\omega_s^{(p)} \to 0$. For small values of $\delta\omega_s^{(p)} < 0.1$, we use the Taylor series expansion

$$a_2 = 1 - \frac{\delta\omega_s^{(p)2}}{6} + \frac{\delta\omega_s^{(p)4}}{120} - O(\delta\omega_s^{(p)6}), \qquad a_3 = \frac{1}{2} - \frac{\delta\omega_s^{(p)2}}{24} + \frac{\delta\omega_s^{(p)4}}{720}\,O(\delta\omega_s^{(p)6}).$$

6. Numerical Results. Below, some numerical results obtained for five test problems of nonlinear deformation of thin plates and shells are given.

6.1. *Pure Bending of a Strip.* A cantilever strip of length L of rectangular cross section with dimensions $b \times h$ is loaded by a tip moment M in the plane of minimum stiffness. The following data of [10] are used (dimensions are not given): $L = 12$, $b = 1$, $h = 0.1$, $E = 12 \cdot 10^5$, $\nu = 0$, and $M_{\max} = 50\pi/3$. Owing to symmetry, a half of the strip is considered using a $n_1 \times n_2$ uniform finite-element mesh shown in Fig. 2 (n_1 and n_2 are mesh spacings along the x_1 and x_2 axes, respectively). The values of the axial displacement u_A and deflection w_A of the strip tip obtained by the finite elements proposed are listed in Table 1. These values are compared with the exact solution

$$u_A = L\Big(1 - \frac{\sin\alpha}{\alpha}\Big), \qquad w_A = L\,\frac{1-\cos\alpha}{\alpha}, \qquad \alpha = \frac{ML}{EI}$$

($I = bh^3/12$ is the cross-sectional moment of inertia), according to which $u_A = 12$ and $w_A = 7.639$ for $M = 0.5M_{\max}$ and $u_A = 12$ and $w_A = 0$ for $M = M_{\max}$. In addition, we give the results obtained in [10] for a 1×16 mesh of rectangular four-node elements with six degrees of freedom per node: $u_A = 12.000$ and $w_A = 7.652$ for $M = 0.5M_{\max}$ and $u_A = 12.000$ and $w_A = 0.000$ for $M = M_{\max}$.

It is worth noting that the large-displacement behavior is well described by the finite element proposed even for coarse meshes. For example, when the strip is bent into a half ring at $M/M_{\max} = 0.5$, the errors in determining the displacements u_A and w_A using a 1×2 mesh (four elements with a side ratio of $12:1$) are only 4.6 and 2.1%, respectively. For coarse meshes, the solution obtained by the finite element of [6] is physically meaningless. One can see from Table 1 that, for a smaller total number of degrees of freedom, the accuracy provided by the finite element considered is not poorer, as compared to the other finite-element models.

TABLE 1

Displacements of the Cantilever Strip under Pure Bending for Different Numbers of Finite Elements

Mesh	u_A		w_A	
	Present solution	Solution [6]	Present solution	Solution [6]
$M/M_{\max} = 0.5$				
1×2	11.445	—	7.802	—
1×5	11.998	12.975	7.640	7.019
1×10	12.001	12.368	7.639	7.411
1×16	12.001	12.273	7.639	7.462
1×20	12.001	12.225	7.639	7.494
$M/M_{\max} = 1.0$				
1×5	12.007	—	0.026	—
1×10	11.996	10.943	0.000	0.349
1×16	11.995	11.462	0.000	0.080
1×20	11.995	11.607	0.000	0.041

TABLE 2

Displacements of the Cantilever Strip under Transverse Bending for Different Numbers of Finite Elements

Mesh	u_A		w_A	
	Present solution	Solution [6]	Present solution	Solution [6]
$P/P_{\max} = 0.5$				
1×2	1.493	1.680	4.707	5.168
1×5	1.592	1.629	4.906	4.986
1×10	1.605	1.640	4.932	4.985
1×16	1.607	1.638	4.935	4.980
1×20	1.607	1.632	4.936	4.971
$P/P_{\max} = 1$				
1×2	3.106	3.756	6.416	7.286
1×5	3.268	3.361	6.665	6.793
1×10	3.287	3.341	6.697	6.749
1×16	3.290	3.334	6.701	6.738
1×20	3.290	3.324	6.701	6.730

6.2. *Transverse Bending of a Strip.* A cantilever strip of length L and rectangular cross section with dimensions $b \times h$ is loaded by a tip shear force P. The finite-element mesh and the distribution law of the nodal load are similar to those considered in Sec. 6.1 (see Fig. 2). The following data of [10] are employed (dimensions of the quantities are not given): $L = 10$, $b = 1$, $h = 0.1$, $E = 12 \cdot 10^5$, $\nu = 0$, and $P_{\max} = 4$. Table 2 gives the tip displacements of the strip u_A and w_A for two values of the load. As the number of finite elements increases, the solution obtained by the finite-element model proposed rapidly converges to the values calculated using the extensible plane rod model [4]: $u_A = 1.606$ and $w_A = 4.935$ for $P = 0.5P_{\max}$ and $u_A = 3.289$ and $w_A = 6.700$ for $P = P_{\max}$. For comparison, we give the results of [10] obtained for a 1×16 mesh of rectangular four-node elements with six degrees of freedom per node: $u_A = 1.604$ and $w_A = 4.933$ for $P = 0.5P_{\max}$ and $u_A = 3.286$ and $w_A = 6.698$ for $P = P_{\max}$. It follows from Table 2 that the element proposed here provides reasonable accuracy for a smaller total number of degrees of freedom.

We note that the displacements calculated by the finite element model of [6] are somewhat overpredicted.

6.3. *Buckling of a Plate.* We consider the buckling problem for a simply supported square plate with side b under uniformly distributed uniaxial compressive loads p. This problem is chosen to verify the interaction between the membrane and bending factors related by nonlinear dependences. The critical load was calculated for the following parameters: $E = 2 \cdot 10^{11}$ N/m^2, $\nu = 0$, $b = 1$ m, and $h = 0.01$ m. Owing to symmetry, a quarter of

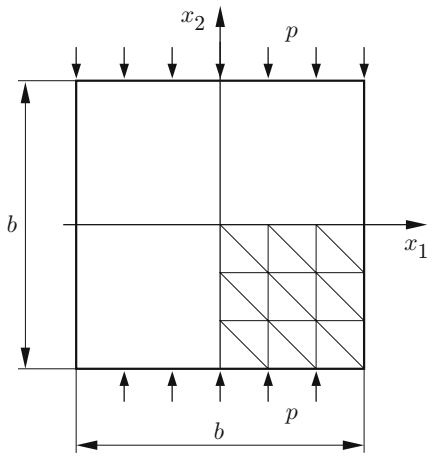

Fig. 3. Square plate under uniaxial compression.

TABLE 3

Parameter of the Critical Load for a Simply Supported Square Plate for Different Numbers of Finite Elements

Mesh	k	
	Present solution	Solution [6]
1×1	3.8499	3.4649
2×2	3.9758	3.8740
3×3	3.9932	3.9436
4×4	3.9978	3.9675

the plate was modeled using a uniform finite-element mesh (Fig. 3). The values of the critical load parameter $k = p_{cr}b^2/(\pi^2 D)$ are listed in Table 3. The exact analytical solution obtained for the classical formulation of the buckling problem yields $k = 4$ [11]. The use of only two elements leads to a small error of 3.8%.

6.4. *Bending of a Spherical Shell.* We consider the problem of nonlinear deformation of a shell shaped like a truncated hemisphere of radius R loaded by two inward and two outward radial forces P (Fig. 4). The following data (dimensions of the quantities are not given) are used [10]: $E = 6.825 \cdot 10^7$, $\nu = 0.3$, $R = 10$, $h = 0.04$, $P_{\max} = 400$, and $\alpha = 18^\circ$ (α is the opening angle of the cutout at the shell pole). Owing to symmetry, a quarter of the shell was modeled using an "isotropic" finite-element mesh (a 8×8 mesh of this type is shown in Fig. 4). The radial displacements of the loaded points are listed in Table 4 versus the load. The displacements predicted by the element proposed converge to somewhat lower values, as compared to those obtained in [10] on a 16×16 mesh of rectangular four-node elements with six degrees of freedom per node (a maximum error of 2.3% in determining w_B is observed at the initial stage of loading).

6.5. *Radial Compression of a Cylindrical Shell.* We consider a circular cylindrical shell of radius R and length L compressed by four radial forces P acting in the plane of the middle cross section of the shell (Fig. 5a). We assume that each loaded node can move only in the radial direction. Thus, we impose eight constraints, which exclude shell motion as a solid. The data of the problem are as follows: $R = 0.1$ m, $L = 0.1$ m, $h = 0.001$ m, $E = 2 \cdot 10^{11}$ N/m^2, and $\nu = 0$. The nonlinear deformation of the shell under kinematic loading, i.e., under the assumption of uniform displacements of all loaded nodes was studied in [6]. It was found that, for a certain load, the shell can exhibit equilibrium configurations characterized by warped cross sections in addition to symmetric four-lobe configurations.

It is of interest to refine the findings of [6] using the finite-element model proposed. In Fig. 5b, the solid curves show the dependence of the loading parameter $\lambda = PR^2/(DL)$ on the deflection w at the loaded node of the shell, which was obtained on an "isotropic" 12×72 mesh comprising 1728 elements and 936 nodes. For comparison, the solution obtained on a 8×48 mesh comprising 768 elements and 432 nodes is also given (dashed curves).

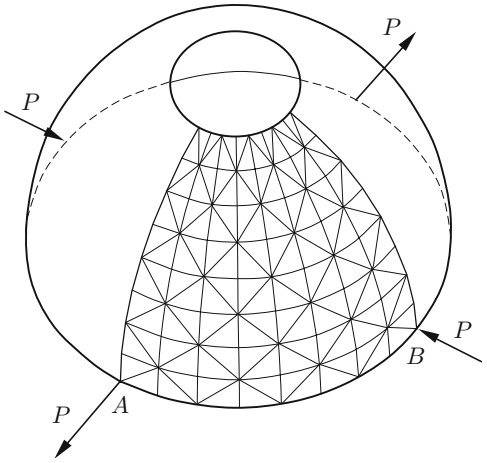

Fig. 4. Hemispherical shell loaded by four radial forces.

TABLE 4

Displacements of the Hemispherical Shell Loaded by Four Forces for Different Numbers of Finite Elements

$P/P_{\max}$	Mesh	w_A	w_B
0.2	8×8	2.342	3.324
	12×12	2.316	3.214
	16×16	2.310 (2.321)	3.190 (3.261)
	20×20	2.310	3.190
0.4	8×8	3.191	5.287
	12×12	3.152	5.114
	16×16	3.143 (3.158)	5.082 (5.196)
	20×20	3.142	5.085
0.6	8×8	3.658	6.660
	12×12	3.604	6.431
	16×16	3.590 (3.598)	6.385 (6.497)
	20×20	3.587	6.383
0.8	8×8	3.981	7.746
	12×12	3.898	7.428
	16×16	3.877 (3.875)	7.360 (7.448)
	20×20	3.871	7.348
1.0	8×8	4.324	8.937
	12×12	4.110	8.225
	16×16	4.080 (4.067)	8.125 (8.178)
	20×20	4.070	8.101

Note. The values in parentheses are obtained in [10].

Calculations show that, for the force-controlled loading, the basic deformation branch contains bifurcation points $B_1, \ldots, B_4$. It is worth noting that similar results were obtained for a narrow ring under the same loading conditions using the finite-element model of a spatial rod [12]. An analysis of the bifurcation points and the corresponding branches of equilibrium states requires much computational work and is out of the scope of the present study; therefore, we confine ourselves to the branches considered in [6]. At the initial stage of deformation OB_1, the shell is stable. Upon attainment of the bifurcation point B_1, buckling of the shell occurs, and the cross sections become shaped like an oval. Provided the loaded nodes approach each other uniformly (kinematic loading), the stable-deformation range extends up to the point B_2 ($\lambda = 10.251$ and $w = 0.118R$), through which the branch of asymmetric equilibrium configurations with warped cross sections passes. Figure 6 shows an example of these configurations for state S (see Fig. 5b) characterized by $\lambda = 18.147$ and $w = 0.495R$.

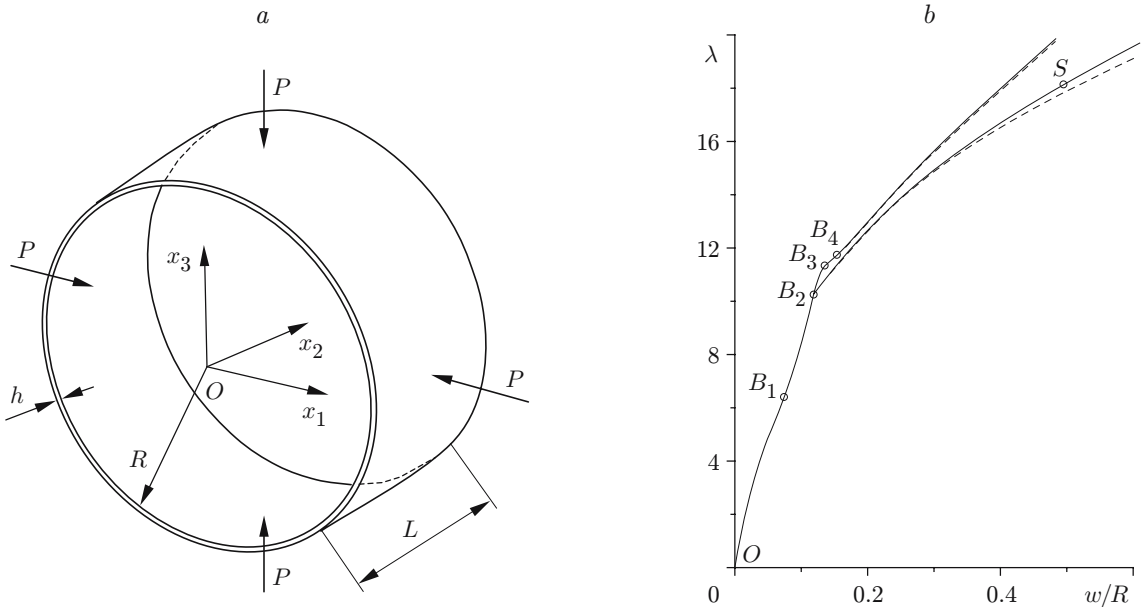

Fig. 5. Cylindrical shell loaded by four radial forces (a) and loading parameter versus deflection (b): the solid and dashed curves refer to the 12×72 mesh and 8×48 mesh, respectively.

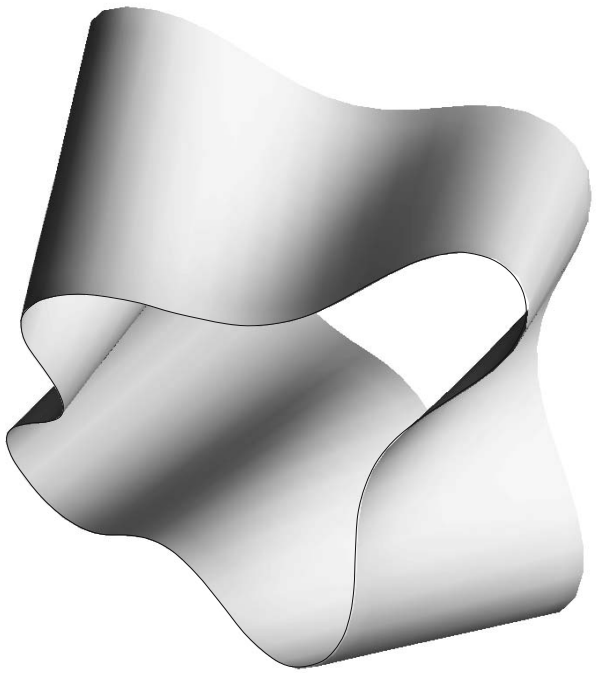

Fig. 6. Postcritical equilibrium configuration of the cylindrical shell compressed by four radial forces.

Conclusions. A new approach to constructing a finite-element model of nonlinear deformation of thin shells, based on the Kirchhoff–Love hypotheses, is proposed. This approach takes into account finite curvature changes within one element and is distinguished for simple formulations of the basic relations. Difficulties arising in application of variation methods to a highly nonlinear system are overcome by using a three-level scheme for calculating variations.

The solution of the test problems shows that considerable improvement of the convergence rate with respect to the number of finite elements has been achieved, as compared with [6]. In view of the fact that triangles are universal elements for modeling surfaces of arbitrary geometry, it can be concluded that the finite element proposed is an effective tool for analysis of nonlinear deformation and stability of thin elastic shells.

REFERENCES

1. S. Klinkel, F. Gruttmann, and W. Wagner, "A robust non-linear solid shell element based on a mixed variational formulation," *Comput. Meth. Appl. Mech. Eng.*, **195**, 179–201 (2006).
2. V. V. Kuznetsov and I. F. Obraztsov, "Engineering applications of invariants in mechanics of thin-walled structures," *Izv. Ross. Akad. Nauk, Mekh. Tverd. Tela*, No. 6, 132–140 (1993).
3. V. V. Kuznetsov and S. V. Levyakov, "Kinematic groups and finite elements in deformable body mechanics," *Izv. Ross. Akad. Nauk, Mekh. Tverd. Tela*, No. 3, 67–82 (1994).
4. V. V. Kuznetsov and S. V. Levyakov, "Geometrically nonlinear models of flexible rods," *Construction Mechanics and Calculation of Buildings* (collected scientific papers) [in Russian], No. 5 (1991), pp. 7–10.
5. S. P. Finikov, *Course on Differential Geometry* [in Russian], Gostekhteoretizdat, Moscow (1952).
6. V. V. Kuznetsov and Yu. V. Soinikov, "Strain analysis of shells for arbitrary displacements by the finite-element method," *Izv. Akad. Nauk SSSR, Mekh. Tverd. Tela*, No. 1, 131–138 (1987).
7. O. Z. Zienkiewicz, *The Finite Element Method*, McGraw–Hill, London (1977).
8. V. V. Kuznetsov, "Recursive relations for the variation coefficients of the energy of nonlinear elastic systems," *Izv. Akad. Nauk SSSR, Mekh. Tverd. Tela*, No. 4, 182–183 (1989).
9. V. V. Kuznetsov, "Determination of arbitrary rotations in nonlinear analysis of thin-walled structures," in: *Design of Structural Elements of Aircraft* [in Russian], Mashinostroenie, Moscow (1990), pp. 59–63.
10. K. Y. Sze, X. H. Liu, and S. H. Lo, "Popular benchmark problems for geometric nonlinear analysis of shells," *Finite Elem. Anal. Des.*, **40**, No. 11, 1551–1569 (2004).
11. A. S. Vol'mir, *Stability of Deformable Systems* [in Russian], Nauka, Moscow (1967).
12. V. V. Kuznetsov and S. V. Levyakov, "Analysis of nonlinear solutions with many singular points in problems of spatial deformation of rods," *J. Appl. Mech. Tech. Phys.*, **39**, No. 6, 949–954 (1998).